Joint Reconstruction of Multitemporal or Multispectral Single-Photon 3D LiDAR Images

JOINT RECONSTRUCTION OF MULTITEMPORAL OR MULTISPECTRAL SINGLE-PHOTON 3D LIDAR IMAGES

Abderrahim Halimi[(1)], *Rachael Tobin*[(1)], *Aongus McCarthy*[(1)],
Jose Bioucas-Dias[(2)], *Stephen McLaughlin*[(1)], *Gerald S. Buller*[(1)]

[(1)] School of Engineering and Physical Sciences, Heriot-Watt University, Edinburgh U.K.
[(2)] Instituto de Telecomunicações and Instituto Superior Técnico, Universidade de Lisboa, Portugal

ABSTRACT

The aim of this paper is to propose a specialized algorithm to process Multitemporal or Multispectral 3D single-photon Lidar images. Of particular interest are challenging scenarios often encountered in real world, i.e., imaging through obscurants such as water, fog or imaging multilayered targets such as target behind camouflage. To restore the data, the algorithm accounts for data Poisson statistics and available prior knowledge regarding target depth and reflectivity estimates. More precisely, it accounts for (a) the non-local spatial correlations between pixels, (b) the spatial clustering of target returned photons and (c) spectral and temporal correlations between frames. An ADMM algorithm is used to minimize the resulting cost function since it offers good convergence properties. The algorithm is validated on real data which show the benefit of the proposed strategy especially when dealing with multi-dimensional 3D data.

Index Terms— 3D Lidar imaging, Poisson statistics, Multispectral/Multitemporal, ADMM, NR3D, collaborative sparsity, non-local TV.

1. INTRODUCTION

Single-photon 3D laser detection and ranging (Lidar) imaging provides high resolution depth information that is required in a range of emerging application areas: for example, navigation of autonomous vehicles requires accurate high-speed imaging of the surrounding scene. This leads to the acquisition of 3D videos which requires the development of specialized algorithms to account for repetitive information. This paper proposes a sophisticated algorithm to process this high-dimensional data while assuming the presence of multiple peaks per-pixel in case the laser beam covers many depth surfaces [1, 2], accounting for photon starved regime in case of fast or long-range imaging [3] and accounting for the presence of obscurants (e.g., turbid media) leading to a high background level [4, 5].

Using a TCSPC-based ranging system in such realistic scenarios requires the introduction of a restoration step to optimize data exploitation. Several methods have been proposed in the literature to deal with some specific cases. The multilayered case has been considered in [1, 6, 7] while considering a costly MCMC method for the former, and faster optimization algorithms for the latter. Solutions to process multispectral 3D data have been proposed in [8, 9] but these methods present some limitations when applied to challenging scenarios involving high background levels or requiring fast processing. Other approaches propose fast reconstruction performance [10, 11] but are only designed to process one 3D data cube and do not account for higher dimensions. This paper propose a unifying solution that covers all these scenarios.

To restore multidimensional images, the proposed approach is based on the minimization of a convex function based on a Poisson likelihood and two regularization terms. Akin to [11], the proposed method exploits multi-resolution information in both regularizing terms, which improve the algorithm's reconstruction properties. The first convex term generalizes [7] by using a non-local total variation (TV) regularization term for reflectivity. The second term uses a collaborative sparse prior to reduce the number of active sub-blocs inside the data cube [12, 13]. In both terms we consider correlations between dimensions while assuming a slight movement of the target for different wavelengths or temporal frames. The resulting formulation is minimized using an alternating direction method of multipliers (ADMM) algorithm [10, 14–16]. The proposed approach is validated on real multi-temporal Lidar data acquired through a dense fog.

The paper is organized as follows. Section 2 introduces the considered statistical model. Section 3 presents our restoration approach and estimation algorithm. Results and conclusions are finally reported in Sections 4 and 5.

2. OBSERVATION MODEL

3D images can be obtained using a Lidar system by sending light pulses and detecting the reflected photons and their time

This work was supported by the UK Royal Academy of Engineering under the Research Fellowship Scheme (RF/201718/17128), EPSRC Grants EP/J015180/1, EP/N003446/1, EP/M01326X/1, EP/K015338/1, EP/S000631/1; the MOD University Defence Research Collaboration (UDRC) in Signal Processing and by the Portuguese Science and Technology Foundation under the Project UID/EEA/50008/2013.

of flight (TOF) from the target for each spatial location/pixel. The data is then represented in three dimensional cube with two spatial dimensions and one dimension representing histogram of photon counts with respect to their TOF. In this paper, we consider a more general case in which the data is acquired on several wavelengths, as in multispectral 3D imaging, or at successive time instants for 3D videos. For both cases, the acquired data can be represented in a four dimensional cube with 3 spatial dimensions and one dimension related to wavelength or time frame. Let $\boldsymbol{y}_{n,t,d}$ be the Lidar observation for the for dth dimension (wavelength, time frame or other) which denotes the number of observed photon counts within the tth TOF bin of the nth pixel, where $n \in \{1, \cdots, N\}$. According to [17, 18], we assume the observed photon counts $\boldsymbol{y}_{n,t,d}$ are drawn from Poisson distribution $\mathcal{P}(.)$ as follow

$$y_{n,t,d} \sim \mathcal{P}(s_{n,t,d}) \tag{1}$$

where

$$s_{n,t,d} = \sum_{m=1}^{M_n} \left[r_{n,m,d}\, g_d\left(t - k_{n,m,d}T\right)\right] + b_{n,d} \tag{2}$$

with M_n denoting the number depth layers in the nth pixel (to cover the case of imaging through camouflage or semi-transparent surfaces), $k_{n,m,d} \geq 0$ and $r_{n,m,d} \geq 0$ are the mth object range's position and reflectivity , respectively, $b_{n,d} \geq 0$ denotes the background and dark counts of the detector, and g_d is the system impulse response (SIR) assumed to be known from a calibration step. It should be noted that the target parameters (reflectivities and depths) depend on the dth dimension to account for the target, system and environment variations between successive images. Similarly, we allow the system impulse response to vary with respect to d as for the case of multi-wavelength imaging. In its discrete version, Eq. (2) can be expressed as a linear system given by [1]

$$\boldsymbol{s}_{n,d} = \boldsymbol{G}_d \boldsymbol{x}_{n,d} \tag{3}$$

where shifted impulse responses are gathered in the $K \times (K+1)$ matrix $\boldsymbol{G}_d = \left[\boldsymbol{g}_d^1, \cdots, \boldsymbol{g}_d^K, \boldsymbol{1}_{K\times 1}\right]$, K being the number of time bins, $\boldsymbol{1}_{i\times j}$ denotes the $(i \times j)$ matrix of 1, $\boldsymbol{g}_d^i = [g_d(T - iT), g_d(2T - iT), \cdots, g_d(KT - iT)]^\top$ is a $(K \times 1)$ vector representing the dth discrete impulse response centered at iT and $\boldsymbol{x}_{n,d}$ is a $(K+1) \times 1$ vector whose value are zero except for $\boldsymbol{x}_{n,d}(k_{n,m,d}) = r_{n,m,d}, \forall m$, and $\boldsymbol{x}_{n,d}(K+1) = b_{n,d}$. Combining (3) and data Poisson statistics, the negative-log-likelihood associated with the discrete observations $\boldsymbol{y}_{n,k,d} \sim \mathcal{P}\left[\left(\boldsymbol{G}_d \boldsymbol{x}_{n,d}\right)_k\right]$ can be evaluated as follows

$$\mathcal{L}_{n,d}\left(\boldsymbol{x}_{n,d}\right) = \mathcal{H}_{n,d}\left(\boldsymbol{G}_d \boldsymbol{x}_{n,d}\right) \tag{4}$$

where $\mathcal{H}_{n,d} : \mathbb{R}^K \to \mathbb{R} \cup \{-\infty, +\infty\}$ is given by

$$\mathcal{H}_{n,d}\left(\boldsymbol{z}\right) = \sum_{k=1}^{K} \left\{ z_k - y_{n,k} \log\left[z_k^{(+)}\right] + i_{\mathbb{R}_+}\left(z_k\right)\right\} \tag{5}$$

where $z_k^{(+)} = \max\{0, z_k\}$ and $i_{\mathbb{R}_+}(x)$ is the indicator function that imposes non-negativity ($i_{\mathbb{R}_+}(x) = 0$ if $x \geq 0$ and $+\infty$ otherwise).

Let $\boldsymbol{Y}$, $\boldsymbol{X}$ be the $N \times K \times D$ matrices gathering all observations of $\boldsymbol{y}_{n,k,d}$ and $\boldsymbol{y}_{n,k,d}$, respectively, and $\boldsymbol{Y}_d$, $\boldsymbol{X}_d$ those associated with the dth dimension. The joint negative joint likelihood is obtained by assuming $\boldsymbol{y}_n$ conditionally independent given $\boldsymbol{X}$, as follows

$$\mathcal{L}\left(\boldsymbol{X}\right) = -\log\left[P(\boldsymbol{Y}|\boldsymbol{X})\right] = \sum_{n,d} \mathcal{L}_{n,d}\left(\boldsymbol{x}_{n,d}\right). \tag{6}$$

The goal is then to estimate the sparse matrices $\boldsymbol{X}_d, \forall d$, while considering that the same target is observed by the different dimensions $d \in \{1, \cdots, D\}$.

3. REGULARIZED PROBLEM

It is necessary to introduce prior knowledge or some regularization terms to the ill-posed problem associated with the estimation of matrix $\boldsymbol{X}$ by minimizing $\mathcal{L}\left(\boldsymbol{X}\right)$. Such regularization will be related to the target depths and reflectivities leading to a new cost function given by

$$\mathcal{C}\left(\boldsymbol{X}\right) = \mathcal{L}\left(\boldsymbol{X}\right) + i_{\mathbb{R}_+}\left(\boldsymbol{X}\right) + \tau_1 \phi_1\left(\boldsymbol{X}\right) + \tau_2 \phi_2\left(\boldsymbol{X}\right) \tag{7}$$

where $\tau_1 > 0$, $\tau_2 > 0$ are two positive constants, $i_{\mathbb{R}_+}\left(\boldsymbol{X}\right) = \sum_{n,k,d} i_{\mathbb{R}_+}\left(x_{n,k,d}\right)$ and ϕ_1, ϕ_2 are two regularization functions enforcing our prior knowledge on depth and reflectivity, respectively. In the following sections and for clarity purposes, we present at first ϕ_1, ϕ_2 assuming only one dimension, then, we generalize the two functions to account for multiple dimensions.

3.1. Depth regularization: priors on data support

The data cube contains photon returns from both the background and the observed targets. As shown in (2), the background returns are spread over the full cube while those of a target are generally clustered. This is a key observation that will be used to define the prior for the support. Note also that in the photon starved regime, the cube is too sparse and better signal to background ratio can be achieved by using downsampled histograms [11]. By combining these observations, we assume group-sparsity of the denoised data cube on a down-sampled image. This means that the returns associated with a target tend to be clustered and sparse. This effect is promoted in this paper by considering an $\ell_{2,1}$ mixed norm [12, 13] which enforces sparsity on small cubes obtained by grouping local pixels and depth bins, as follows

$$\phi_1\left(\boldsymbol{X}_d\right) = ||\text{diag}(\boldsymbol{v})\boldsymbol{K}\boldsymbol{F}\boldsymbol{X}_d(:)||_{2,1} \tag{8}$$

where $\boldsymbol{X}_d(:) \in \mathbb{R}^{(K+1)N\times 1}$ denotes the vectorization of the matrix $\boldsymbol{X}_d$, $\boldsymbol{F} \in \mathbb{R}^{KN\times(K+1)N}$ is an operator that discards the last background row of $\boldsymbol{X}$ to only select its first K rows, $\boldsymbol{K} : \mathbb{R}^{KN\times 1} \to \mathbb{R}^{S_b \times N_B}$ is a linear operator

that splits the data cubes into N_B small blocs each of size $S_b = (r_b \times c_b \times t_b)$, and $\boldsymbol{v} \in \mathbb{R}^{N_B \times 1}$ contains weights for each bloc. One can also express $\phi_1(\boldsymbol{X})$ as follows

$$\phi_1(\boldsymbol{X}) = \sum_{i=1}^{N_B} v_i \sqrt{\left(\sum_{(t,n)\in\nu_i} x_{n,t}^2 \right)} \tag{9}$$

where ν_i gathers the location information of the ith bloc, i.e., pixel and time-bin indices .

3.2. Regularized intensity: priors on the counts

The photon counts associated with target are restored by accounting for non-local spatial correlation between pixels, as for most state-of-the-art algorithms [19–21]. These correlations should be enforced on informative photons associated with target thus the need for a strategy to separate signal from background counts. As highlighted in [7, 11], low-pass filtered histograms is a good solution as it improves the separation between target and background counts, and it allows to deal with the photon starved regime for which the data cube is too sparse. Therefore, we apply a non-local TV regularization on low-pass filtered image, where each pixel gathers weighted information from similar pixels in the image to improve its estimate, i.e.,

$$\phi_2(\boldsymbol{X}_d) = ||\boldsymbol{H}_w \boldsymbol{D}_h \boldsymbol{F} \boldsymbol{X}_d(:)||_F^2 \tag{10}$$

where $\boldsymbol{D}_h \in \mathbb{R}^{K_h N \times KN}$ is performing a range downsampling by summing each $\#h$ successive time bins, K_h represents the number of resulting blocs given by the integer part of the division K/h, $\boldsymbol{H}_w \in \mathbb{R}^{n_d K_h N \times K_h N}$ computes weighted differences between each pixel and other n_d pixels located in a fixed field (e.g., this is a block-circulant-circulant-block matrix useful for fast computations). More precisely, the operator $\boldsymbol{H}_w : \mathbb{R}^{K_h N} \to \mathbb{R}^{n_d K_h N}$ performs the following operation

$$||\boldsymbol{H}_w \boldsymbol{z}||_F^2 = \sum_{n=1}^{N} \sum_{i=1}^{n_d} \sum_{\ell=1}^{K_h} w_{i,n}^2 \left(H_i^{\text{Diff}} \boldsymbol{z}_\ell \right)^2 \Big|_n \tag{11}$$

where $\boldsymbol{Z} = [\boldsymbol{z}_1, ..., \boldsymbol{z}_{K_h}] \in \mathbb{R}^{N \times K_h}$ is built from $\boldsymbol{z} \in \mathbb{R}^{K_h N}$ and $\boldsymbol{z}_\ell \in \mathbb{R}^N$ denotes its ℓth column. For each pixel, we consider n_d predefined directions, for which we associate the weights $w_{i,n}^2$ for the nth pixel and ith direction, and the operator $H_i^{\text{Diff}} \in \mathbb{R}^{N \times N}$ computing the difference between each pixel and that located at the ith direction. For simplicity, we treat the matrices H_i^{Diff} with periodic boundary conditions as cyclic convolutions.

3.3. Generalization to multidimensional data

Each dimension can be processed independently, however, joint processing will account for complementary information between dimensions to improve performance. We assume that the multidimensional data corresponds to the same scene with a slight movement of the observed object or the camera as considered in many studies [22, 23]. Under this assumption, we might assume that the support of the downsampled images is almost the same leading to

$$\Phi_1(\boldsymbol{X}) = \sum_{i=1}^{N_B} v_i \sqrt{\left(\sum_{d=1}^{D} \sum_{(t,n)\in\psi_i} x_{n,d,t}^2 \right)}. \tag{12}$$

Similarly, the intensity regularization can be defined as

$$\Phi_2(\boldsymbol{X}) = \sum_{d=1}^{D} ||\boldsymbol{H}_w \boldsymbol{D}_h \boldsymbol{F} \boldsymbol{X}_d(:)||_F^2. \tag{13}$$

Note that spatial correlation is promoted between the pixels belonging to the same dimension, as different dimensions might have different intensity responses (e.g. multispectral imaging). Also note that this term introduces correlation between dimensions as we assume the same weights $\boldsymbol{w}$ (that can obtained using all dimensions) for all of them. However, the independent case can be easily obtained by associating a different vector $\boldsymbol{w}_d$ with each dimension.

3.4. Choice of the algorithm parameters

The weights $\boldsymbol{w}, \boldsymbol{v}$ should reflect our prior knowledge about possible spatial correlations and target's depths and can be fixed using complimentary imaging modalities of the same scene leading to a fusion task. In this work, these weights have been fixed using only the Lidar data as described in [24]. The regularization parameters τ_1, τ_2 can be estimated using a Bayesian approach or automated algorithms [25]. In this paper, a grid search is performed and those parameters providing best performance are considered.

3.5. Estimation algorithm

Several strategies can applied to minimize the resulting convex cost function in (7), where most of them are based on dividing the problem into simpler sub-problems [26]. The ADMM algorithm described in [27] is considered in this work as it showed good results in several applications [10, 28]. The algorithm is not described here for brevity and we invite the reader to consult [26, 27] for more details.

4. RESULTS ON REAL MULTITEMPORAL DATA ACQUIRED THROUGH OBSCURANTS

4.1. Data description

This section evaluates the proposed algorithm on real data when imaging through obscurants, i.e., in presence of a high

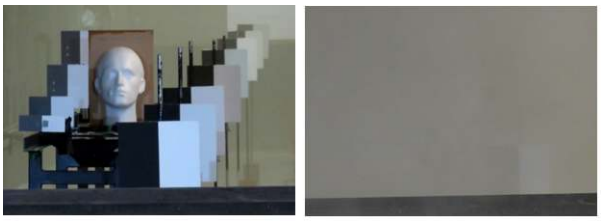

Fig. 1. Picture of the mannequin target: (left) in air, (right) in presence of fog.

background level. The scene considered, consists of a life-sized polystyrene head as shown in Fig. 1, and was set in a fog chamber (of dimensions $26 \times 2.5 \times 2.3$ meters) located in an indoor facility at the French-German Research Institute of Saint-Louis (ISL). The target was located at a distance of 21.5 m from the sensor, and 5 m inside the fog chamber. To study the effect of different fog levels, the chamber was filled with water fog with a high density, then a succession of 3D images were taken as the fog density decreased. The data were acquired every 60 s, where each image contains 92×67 pixels and 400 time bins, and was acquired during 30 seconds (i.e., 3 ms acquisition time per pixel). This provides successive data cubes with decreasing fog level, i.e., background level.

4.2. Algorithms

The proposed algorithm, denoted Multidimensional-Nonlocal Restoration of 3D (M-NR3D) images or just NR3D when applied to a independent data cube, is run using $(r_b, c_b, t_b, h) = (4, 4, 50, 5)$. The NR3D regularization parameters are manually selected to provide best qualitative performance when testing the following intervals $\tau_1 = (1, 10, 100)$ and $\tau_2 = (0.01, 0.1, 1)$. The algorithm is compared to:

- The classical algorithm that computes maximum likelihood estimates of the depth and reflectivity maps while assuming the presence of one peak per pixel and no background noise
- RDI-TV algorithm [10] computes maximum-a-posteriori estimates while considering a TV regularization term and no background noise. It is assumed that the position of missing pixels is known and that there is only one peak per pixel
- TV-ℓ_{21} algorithm [7] which generalizes RDI-TV by accounting for the presence of multiple peaks and is designed to reconstruct scenes presenting objects well separated in the depth dimension, as for the proposed mannequin face target.

Except M-NR3D, all described algorithms process the cubes independently.

4.3. Discussion

Fig. 2 show the point clouds obtained using different algorithms for three time instants, where the fog density decreases from T_1 to T_3. Note that depth is represented by the point locations and reflectivity is colour coded. All algorithms perform well in presence of a low fog density, as shows for T_3. However, the advantage of both TV-ℓ_{21} and NR3D with respect to Classical and RDI-TV becomes clear in presence of a dense fog (see T_1) since they better exploit the spatial correlation of the histograms. Thanks to its joint processing of the three datasets (T_1, T_2 and T_3), M-NR3D performs the best and the mannequin face is reconstructed even for the extreme case T1. This highlights the importance of the joint processing of multidimensional data.

5. CONCLUSIONS

A new optimization based algorithm is presented to restore single-photon 3D images under challenging scenarios. The algorithm allows the restoration of data acquired in the photon starved regime or in presence of a high background noise due to obscurants. A generalization for the joint processing of high-dimensional data is presented and was shown to improve reconstruction performance. Future work includes the consideration of other simulation scenarios to highlight the algorithm capabilities (e.g., multiple peaks per pixel). Setting the weights using other imaging modalities is also very interesting and will be investigated in the future to perform multi-modality data fusion.

6. REFERENCES

[1] D. Shin, F. Xu, F. N. C. Wong, J. H. Shapiro, and V. K. Goyal, "Computational multi-depth single-photon imaging," *Opt. Express*, vol. 24, no. 3, pp. 1873–1888, Feb 2016.

[2] R. Tobin, A. Halimi, A. McCarthy, X. Ren, K. J. McEwan, S. McLaughlin, and G. S. Buller, "Long-range depth profiling of camouflaged targets using single-photon detection," *Optical Engineering*, vol. 57, pp. 031 303 (1–10), 2017.

[3] A. M. Pawlikowska, A. Halimi, R. A. Lamb, and G. S. Buller, "Single-photon three-dimensional imaging at up to 10 kilometers range," *Opt. Express*, vol. 25, no. 10, pp. 11 919–11 931, May 2017.

[4] A. Maccarone, A. McCarthy, X. Ren, R. E. Warburton, A. M. Wallace, J. Moffat, Y. Petillot, and G. S. Buller, "Underwater depth imaging using time-correlated single-photon counting," *Opt. Express*, vol. 23, no. 26, pp. 33 911–33 926, Dec 2015.

[5] A. Halimi, A. Maccarone, A. McCarthy, S. McLaughlin, and G. S. Buller, "Object depth profile and reflectivity restoration from sparse single-photon data acquired in underwater environments," *IEEE Trans. Comput. Imaging*, vol. 3, no. 3, pp. 472–484, 2017.

[6] S. Hernandez-Marin, A. M. Wallace, and G. J. Gibson, "Multilayered 3D lidar image construction using spatial models in a bayesian framework," *IEEE Trans. Pattern Anal. Mach. Intell.*, vol. 30, no. 6, pp. 1028–1040, June 2008.

[7] A. Halimi, R. Tobin, A. McCarthy, S. McLaughlin, and G. S. Buller, "Restoration of multilayered single-photon 3D lidar images," in *Proc. EUSIPCO*, 2017, pp. 708–712.

[8] Y. Altmann, A. Maccarone, A. Halimi, A. McCarthy, G. Buller, and S. McLaughlin, "Efficient range estimation and material quantification from multispectral lidar waveforms," in *2016 Sensor Signal Processing for Defence (SSPD)*, Sept 2016, pp. 1–5.

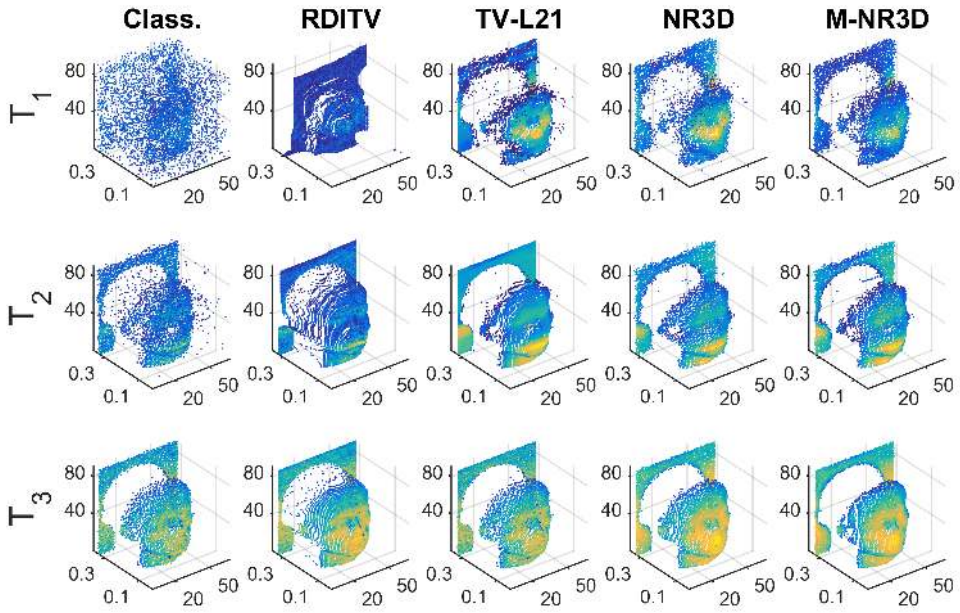

Fig. 2. Cloud points (92×67 pixels) of a life-sized polystyrene head acquired under different level of water fog. (First column) classical cross-correlation, (second column) RDI-TV, (third column) TV-L21, (fourth column) proposed NR3D algorithm, (fifth column) proposed M-NR3D algorithm. Reflectivity is colour coded.

[9] X. Ren, Y. Altmann, R. Tobin, A. Mccarthy, S. Mclaughlin, and G. S. Buller, "Wavelength-time coding for multispectral 3d imaging using single-photon lidar," *Opt. Express*, vol. 26, no. 23, pp. 30 146–30 161, Nov 2018.

[10] A. Halimi, Y. Altmann, A. McCarthy, X. Ren, R. Tobin, G. S. Buller, and S. McLaughlin, "Restoration of intensity and depth images constructed using sparse single-photon data," in *Proc. EUSIPCO*, 2016, pp. 86–90.

[11] J. Rapp and V. K. Goyal, "A few photons among many: Unmixing signal and noise for photon-efficient active imaging," *IEEE Trans. Comput. Imaging*, vol. 3, no. 3, pp. 445–459, Sept. 2017.

[12] P. Sprechmann, I. Ramirez, G. Sapiro, and Y. C. Eldar, "C-Hilasso: A collaborative hierarchical sparse modeling framework," *IEEE Trans. Signal Process.*, vol. 59, no. 9, pp. 4183–4198, Sept 2011.

[13] M. D. Iordache, J. M. Bioucas-Dias, and A. Plaza, "Collaborative sparse regression for hyperspectral unmixing," *IEEE Trans. Geosci. Remote Sens.*, vol. 52, no. 1, pp. 341–354, Jan 2014.

[14] S. Boyd, N. Parikh, E. Chu, B. Peleato, and J. Eckstein, "Distributed optimization and statistical learning via the alternating direction method of multipliers," *Found. Trends Mach. Learn.*, vol. 3, no. 1, pp. 1–122, Jan 2011.

[15] M. Figueiredo and J. Bioucas-Dias, "Restoration of Poissonian images using alternating direction optimization," *IEEE Trans. Image Process.*, vol. 19, no. 12, pp. 3133–3145, Dec 2010.

[16] M.-D. Iordache, J. Bioucas-Dias, and A. Plaza, "Total variation spatial regularization for sparse hyperspectral unmixing," *IEEE Trans. Geosci. Remote Sens.*, vol. 50, no. 11, pp. 4484–4502, Nov. 2012.

[17] S. Hernandez-Marin, A. Wallace, and G. Gibson, "Bayesian analysis of Lidar signals with multiple returns," *IEEE Trans. Pattern Anal. Mach. Intell.*, vol. 29, no. 12, pp. 2170–2180, Dec. 2007.

[18] Y. Altmann, X. Ren, A. McCarthy, G. S. Buller, and S. McLaughlin, "Lidar waveform based analysis of depth images constructed using sparse single photon data," *IEEE Trans. Image Process.*, vol. 25, no. 5, pp. 1935–1946, Mar. 2015.

[19] A. Buades, B. Coll, and J. M. Morel, "A review of image denoising algorithms, with a new one," *Multiscale Modeling & Simulation*, vol. 4, no. 2, pp. 490–530, 2005.

[20] K. Dabov, A. Foi, V. Katkovnik, and K. Egiazarian, "Image denoising by sparse 3-D transform-domain collaborative filtering," *IEEE Trans. Image Process.*, vol. 16, no. 8, pp. 2080–2095, Aug 2007.

[21] J. Salmon, Z. Harmany, C.-A. Deledalle, and R. Willett, "Poisson noise reduction with non-local PCA," *Journal of Mathematical Imaging and Vision*, vol. 48, no. 2, pp. 279–294, 2014.

[22] A. Halimi, N. Dobigeon, J. Y. Toumeret, S. McLaughlin, and P. Honeine, "Unmixing multitemporal hyperspectral images accounting for endmember variability," in *Proc. EUSIPCO*, Aug 2015, pp. 1656–1660.

[23] S. Henrot, J. Chanussot, and C. Jutten, "Dynamical spectral unmixing of multitemporal hyperspectral images," *IEEE Trans. Image Process.*, vol. 25, no. 7, pp. 3219–3232, July 2016.

[24] A. Halimi, X. Ren, A. McCarthy, J. Bioucas-Dias, S. McLaughlin, and G. S. Buller, "Restoration of multilayered single-photon 3d lidar images," in *IEEE Sensor Array and Multichannel Signal Processing Workshop (SAM)*, July 2018, pp. 1–5.

[25] C. Deledalle, S. Vaiter, J. Fadili, and G. Peyre, "Stein unbiased gradient estimator of the risk (SUGAR) for multiple parameter selection," *SIAM Journal on Imaging Sciences*, vol. 7, no. 4, pp. 2448–2487, 2014.

[26] L. Boyd, Sand Vandenberghe, *Convex Optimization*. New York, NY, USA: Cambridge University Press, 2004.

[27] M. Afonso, J. Bioucas-Dias, and M. Figueiredo, "An augmented lagrangian approach to the constrained optimization formulation of imaging inverse problems," *IEEE Trans. Image Process.*, vol. 20, no. 3, pp. 681–695, March 2011.

[28] A. Halimi, J. M. Bioucas-Dias, N. Dobigeon, G. S. Buller, and S. McLaughlin, "Fast hyperspectral unmixing in presence of nonlinearity or mismodeling effects," *IEEE Transactions on Computational Imaging*, vol. 3, no. 2, pp. 146–159, June 2017.